Simen Owen Academic Proceedings Series

Vol. 3 2026

Article **Open Access**

Improving Ionic Conductivity and Interface Stability in All-Solid-State Batteries Using Nanocomposite Solid Electrolytes

Ruiqi Zhao [1,*]

[1] Tianjin Sino-German University of Applied Sciences, Tianjin, 300350, China
* Correspondence: Ruiqi Zhao, Tianjin Sino-German University of Applied Sciences, Tianjin, 300350, China

Abstract: All-solid-state batteries (ASSBs) have emerged as promising candidates for next-generation energy storage due to their intrinsic safety and compatibility with high-energy-density lithium metal anodes. However, their commercialization is hindered by two persistent bottlenecks: the relatively low ionic conductivity of solid electrolytes compared to liquids and the instability of electrode-electrolyte interfaces. Existing approaches often improve one aspect in isolation but fail to simultaneously optimize both properties under practical cycling conditions. In this study, we propose an in situ-assembled nanocomposite solid electrolyte, where oxide nanoparticles are homogeneously dispersed within a sulfide-based host matrix through a sol-gel assisted synthesis. This design integrates percolation pathways that reduce activation energy for Li^+ transport and introduces a nanoscale passivation layer that suppresses interfacial side reactions. Electrochemical tests demonstrate a room-temperature ionic conductivity of 1.7×10^{-3} S·cm^{-1}, a 2.3-fold improvement over pure sulfide and a 6.1-fold improvement over oxide baselines. Interfacial resistance was reduced to 18 Ω·cm^2, and full-cell cycling retained 91% capacity after 300 cycles. Ablation and robustness studies further confirm the critical role of filler concentration, particle size, and interfacial engineering. These results establish a reproducible framework for enhancing both conductivity and interfacial stability in ASSBs. The proposed nanocomposite design provides a scalable pathway toward safer, high-performance solid-state batteries, directly supporting future applications in electric vehicles and grid-scale energy storage.

Keywords: all-solid-state batteries; nanocomposite solid electrolytes; ionic conductivity; interface stability; sol-gel synthesis

Received: 06 December 2025
Revised: 27 January 2026
Accepted: 10 February 2026
Published: 17 February 2026

Copyright: © 2026 by the authors. Submitted for possible open access publication under the terms and conditions of the Creative Commons Attribution (CC BY) license (https://creativecommons.org/licenses/by/4.0/).

1. Introduction

The rapid growth of electric vehicles, grid-scale storage, and portable electronics has driven the demand for safer and higher-energy-density batteries. All-solid-state batteries (ASSBs) are increasingly viewed as the most promising successor to conventional lithium-ion batteries, since they eliminate flammable organic liquid electrolytes, enable the use of lithium metal anodes, and offer superior thermal stability [1]. Despite these inherent advantages, the large-scale implementation of ASSBs remains hampered by two interrelated problems: the relatively low ionic conductivity of solid-state electrolytes compared with liquid systems, and the poor interfacial stability at the electrode-electrolyte contact [2]. Both limitations directly reduce energy efficiency, rate capability, and cycle life, thereby preventing the transition from laboratory demonstration to commercial deployment.

Over the past decade, several families of solid electrolytes have been explored. Sulfide-based electrolytes provide high ionic conductivity in the range of 10^{-3} to 10^{-2} S cm^{-1}, yet their intrinsic chemical instability against moisture and lithium metal often

causes severe degradation and interfacial side reactions [3]. Oxide-based electrolytes, such as garnet-type and NASICON-type materials, exhibit wider electrochemical stability windows and robust structural frameworks, but their conductivities typically fall below 10^{-4} S cm^{-1} at room temperature, and they suffer from significant grain-boundary resistance [4]. More recently, halide electrolytes have gained attention for their favorable balance between ionic transport and stability; however, their cycling durability and compatibility with high-voltage electrodes remain under scrutiny [5]. These trade-offs illustrate that no single electrolyte class has yet achieved the dual requirements of high conductivity and long-term interface stability [6].

In order to bridge this gap, hybrid and nanocomposite strategies have emerged as a compelling direction. By incorporating nanoscale fillers into a host matrix, nanocomposite solid electrolytes can create percolation pathways that enhance lithium-ion mobility, while simultaneously modifying the interface to suppress unfavorable reactions. Recent studies have shown measurable improvements in either conductivity or interface behavior, but most of them focus on one aspect in isolation and rarely demonstrate comprehensive optimization of both. Furthermore, many reported approaches are limited to short-term cycling or narrowly defined conditions, leaving open questions regarding robustness under varied current densities, temperatures, and long-term operation.

The present study addresses these challenges by proposing a novel in situ-assembled nanocomposite solid electrolyte architecture. Oxide nanoparticle fillers are homogeneously dispersed within a sulfide-based host using a controlled sol-gel-assisted assembly process. This design is intended to accomplish two complementary goals: first, to establish continuous and low-tortuosity pathways for lithium-ion conduction, thereby reducing activation energy; and second, to form a thin passivating interfacial layer that minimizes side reactions and stabilizes contact with electrodes. To validate this approach, we combine structural characterization techniques such as X-ray diffraction, transmission electron microscopy, and Raman spectroscopy with electrochemical evaluation, including impedance spectroscopy, DC polarization, and long-term cycling tests. Ablation experiments, in which filler type and concentration are systematically varied, further provide mechanistic insights into the conduction pathways and interfacial behavior.

From an academic perspective, this work contributes to the rational design principles of nanocomposite solid electrolytes, integrating transport modeling, controlled synthesis, and multi-dimensional evaluation. From a practical standpoint, the proposed framework offers a route to simultaneously achieve higher ionic conductivity and stable electrode-electrolyte interfaces, which are both critical to enabling reliable, large-scale ASSB deployment. By addressing these two fundamental bottlenecks in a unified design, the study advances the field toward bridging the persistent gap between laboratory-scale prototypes and real-world applications.

2. Related Works

2.1. Sulfide-Based Electrolytes

Sulfide electrolytes have been extensively studied due to their intrinsically high lithium-ion conductivity, which can reach values in the range of 10^{-3} to 10^{-2} S·cm^{-1} at room temperature. Structural flexibility and soft anion lattices facilitate rapid ion migration, making them suitable for high-rate applications [7]. However, their practical adoption is hindered by significant chemical instability when exposed to ambient moisture and reactivity against metallic lithium and high-voltage cathodes [8]. This leads to the formation of resistive interphases and gas evolution, severely compromising long-term cycling. Although protective coatings and compositional tuning have been employed, these measures often increase manufacturing complexity and do not fully resolve interfacial degradation [9]. For this reason, sulfide electrolytes are powerful benchmarks in conductivity studies but remain inadequate as a stand-alone solution.

2.2. Oxide-Based Electrolytes

Oxide electrolytes, particularly garnet-type and NASICON-type materials, provide wider electrochemical stability windows and robust structural frameworks that tolerate high-voltage cathodes [10]. Their conductivities, however, typically range from 10^{-5} to 10^{-4} S·cm^{-1}, which is significantly lower than sulfide systems. The main bottleneck arises from grain boundary resistance and poor densification during processing [11]. Techniques such as high-temperature sintering, dopant engineering, and interface modification have been employed to address these limitations. While these approaches modestly improve conductivity and reduce interfacial impedance, they often require energy-intensive fabrication methods, limiting scalability [12]. Oxide electrolytes therefore offer stability advantages but need conductivity enhancement strategies to become viable for practical applications.

2.3. Nanocomposite and Hybrid Electrolytes

Nanocomposite electrolytes integrate the advantages of multiple phases by embedding nanoscale fillers into a host matrix [13]. This design can simultaneously enhance ion transport through percolation pathways and stabilize electrode interfaces by modifying local chemical environments. Reported systems have demonstrated conductivity improvements up to 2–3 times compared to single-phase electrolytes, with some achieving values above 10^{-3} S·cm^{-1} at room temperature. Furthermore, nanocomposites exhibit reduced interfacial resistance, sometimes below 20 Ω·cm^2, due to passivation effects. Nonetheless, the effectiveness of these designs strongly depends on filler type, particle dispersion, and interfacial compatibility [14]. Poorly controlled architectures may introduce additional scattering sites or mechanical stress. Compared to sulfide and oxide systems, nanocomposites offer a more balanced trade-off between conductivity and stability (Table 1), aligning closely with the goals of this work [15].

Table 1. Comparative Summary.

Electrolyte Type	Typical Conductivity (S·cm^{-1}, RT)	Strengths	Weaknesses	Relevance to This Work
Sulfide-Based	10^{-3} - 10^{-2}	High conductivity, flexible lattice	Moisture sensitivity, unstable interfaces	Serves as conductivity benchmark
Oxide-Based	10^{-5} - 10^{-4}	Stable, wide electrochemical window	Low conductivity, grain boundary issues	Provides stability reference
Nanocomposite/ Hybrid	≥10^{-3} (with fillers)	Synergistic conduction, stable interfaces	Sensitive to filler dispersion and compatibility	Directly informs proposed approach

By analyzing these three subfields, it becomes evident that no single material family alone meets the dual requirements of high ionic conductivity and stable interfaces. Sulfides excel in conductivity but suffer instability, oxides ensure stability but lack conductivity, and nanocomposites strike a balance but require careful design. This study builds on these insights by proposing an in situ-assembled nanocomposite framework aimed at achieving both enhanced ion transport and robust interfacial stability under practical cycling conditions.

3. Methodology

3.1. Overall Framework

The proposed methodology aims to design and validate a nanocomposite solid electrolyte that simultaneously enhances ionic conductivity and stabilizes electrode interfaces. The strategy combines three essential components: (i) constructing percolation-assisted ion transport networks by embedding oxide nanoparticles into a sulfide-based matrix; (ii) employing a sol-gel-assisted in situ assembly process to ensure homogeneous dispersion and phase compatibility; and (iii) engineering a passivating interfacial layer to suppress side reactions and minimize interfacial resistance. Together, these steps integrate material design, synthesis, and electrochemical evaluation into a coherent framework, ensuring both methodological clarity and experimental reproducibility.

3.2. Core Design Principles

3.2.1. Ionic Percolation Model

The conductivity of solid electrolytes is governed by percolation theory, where the addition of oxide nanoparticles reduces tortuosity and generates fast-conduction pathways. The effective ionic conductivity (σ_eff) is described as:

$$\sigma_{eff} = \sigma_0 \left(1 - \frac{\phi_c}{\phi - \phi_c}\right)^t, \phi > \phi_c \quad (1)$$

where σ_0 is the intrinsic conductivity of the matrix, ϕ is the filler volume fraction, ϕ_c is the critical percolation threshold, and t is the critical exponent (typically 1.6-2.0).

3.2.2. Interfacial Impedance

The resistance at the electrode-electrolyte interface is modeled using an equivalent circuit with charge-transfer resistance and double-layer capacitance. The impedance Z(ω) is:

$$Z(\omega) = R_b + \frac{R_{ct}}{1 + j\omega R_{ct} C_{dl}} \quad (2)$$

where R_b is bulk resistance, R_{ct} is charge-transfer resistance, and C_{dl} is double-layer capacitance.

3.2.3. Ionic Diffusion

The lithium-ion diffusion coefficient (D_{Li}) is derived from the Warburg impedance slope in electrochemical impedance spectroscopy:

$$D_{Li} = \frac{2A^2 n^4 F^4 C^2 \sigma_W^2}{R^2 T^2} \quad (3)$$

where R is gas constant, T is temperature, A is electrode area, n is charge number, F is Faraday constant, C is ion concentration, and σ_W is the Warburg coefficient.

3.2.4. Arrhenius Behavior

The temperature dependence of conductivity follows the Arrhenius law:

$$\sigma(T) = \sigma_\infty \exp\left(-\frac{E_a}{k_B T}\right) \quad (4)$$

where σ_∞ is pre-exponential factor, E_a is activation energy, and k_B is Boltzmann constant.

3.3. Sol-Gel Assisted In Situ Assembly

The sol-gel process is adopted in this work to achieve homogeneous dispersion of oxide fillers within the sulfide electrolyte matrix. Compared with mechanical mixing, which often introduces particle aggregation and heterogeneous interfaces, the sol-gel method enables molecular-level precursor mixing and controlled nanoparticle nucleation. The process involves hydrolysis of metal alkoxides or inorganic salts, formation of colloidal suspensions, gelation into a continuous three-dimensional network, and

subsequent low-temperature annealing to crystallize nanoparticles. This sequence allows in situ growth of oxide nanophases directly inside the sulfide host, ensuring coherent interfaces and improved compatibility.

Key advantages of the sol-gel method include its ability to confine particle sizes within the 5-20 nm range, reduce ion-blocking effects, and provide uniform percolation pathways for lithium-ion transport. Furthermore, it enables structural tuning by adjusting parameters such as precursor concentration, solvent composition, and drying conditions. Control of these variables influences porosity and interparticle connectivity, which directly affect conduction tortuosity and bulk conductivity. Importantly, the process avoids the high sintering temperatures typically required for oxides, lowering energy costs and enhancing scalability.

The gelation kinetics can be described by an Arrhenius relationship:

$$k_{gel} = A \exp\left(-\frac{E_{a,gel}}{RT}\right) \quad (5)$$

where A is the pre-exponential factor, $E_{a,gel}$ is the activation energy, R is the gas constant, and T is absolute temperature. A moderate k_{gel} ensures uniform dispersion without uncontrolled aggregation, providing reliable nanocomposite formation.

3.4. Interface Passivation Layer

Although nanocomposite electrolytes improve bulk conductivity, interfacial stability is equally critical for long-term cycling. To mitigate electrode-electrolyte incompatibility, a nanoscale oxide-rich passivation layer is incorporated. This layer acts as a chemically inert barrier that suppresses decomposition of sulfide species at high-voltage cathodes or against lithium metal anodes. By preventing direct chemical contact, it reduces parasitic side reactions, lowers impedance growth, and extends battery lifetime.

The design principle emphasizes minimal thickness (5-10 nm) to maintain high Li^+ conductivity while blocking electronic leakage. Its composition ensures low electronic conductivity and high chemical stability, creating an optimized balance between transport and protection. This approach allows the interfacial resistance to remain low while ensuring stable operation under varied current densities and temperatures.

The thermodynamic driving force for side reactions is defined as:

$$\Delta G_{rxn} = \Delta G_{interface} + \Delta\Phi \cdot q \quad (6)$$

where $\Delta G_{interface}$ is the intrinsic interfacial Gibbs free energy, $\Delta\Phi$ is the work-function difference, and q is ionic charge. A positive ΔG_{rxn} indicates suppressed side reactions. Long-term stability is evaluated by the time-dependent growth of interfacial resistance:

$$R_{int}(t) \leq R_0 \exp(\alpha t) \quad (7)$$

where R_0 is the initial resistance and α is the degradation coefficient. A smaller α reflects stronger passivation and more durable interfaces.

3.5. Performance Evaluation Models

To quantitatively assess the effectiveness of the proposed nanocomposite solid electrolyte, a performance evaluation framework is established that integrates both bulk transport and interfacial behavior. The total ionic conductivity is expressed as the sum of bulk and interfacial contributions:

$$\sigma_{total} = \sigma_{bulk} + \beta \cdot \sigma_{interface} \quad (8)$$

where σ_{bulk} represents conductivity through the matrix, $\sigma_{interface}$ accounts for enhanced interfacial transport, and β is a coupling coefficient determined by filler-matrix compatibility. This relation captures the synergistic effect of nanoparticle networks and passivation layers.

Evaluation focuses on several key metrics. First, ionic conductivity is measured using AC impedance spectroscopy, with Arrhenius fitting used to extract activation energy values. Second, interfacial resistance is monitored during long-term cycling to determine the degradation coefficient (α) defined earlier, which reflects the rate of impedance

growth. Third, lithium-ion diffusion coefficients are obtained from the Warburg slope in impedance spectra, providing insight into long-range ion mobility. Together, these parameters offer a multidimensional view of the electrochemical behavior of nanocomposite electrolytes.

In addition to these general metrics, structural variables play a decisive role in determining performance. Studies have shown that filler volume fractions between 0.05 and 0.20 are sufficient to trigger percolation, enhancing conductivity without introducing excessive scattering centers. Particle sizes in the range of 10-20 nm enable uniform dispersion, which lowers interfacial resistance compared with larger filler sizes. Likewise, the introduction of a thin oxide-rich passivation layer with a thickness of 5-10 nm has been found to suppress interfacial side reactions while avoiding additional transport barriers. By correlating such structural parameters with electrochemical outputs, the evaluation framework ensures that design choices are not only guided by conductivity improvements but are also aligned with the requirements of interfacial stability and long-term cycling reliability. This systematic approach provides a reproducible basis for optimizing nanocomposite design under diverse operating conditions.

4. Results and Analysis

4.1. Experimental Setup and Dataset

The proposed nanocomposite solid electrolyte was synthesized via a sol-gel assisted in situ assembly process, where oxide nanoparticles (10-15 nm ZrO_2) were incorporated into a Li_6PS_5Cl sulfide matrix at varying volume fractions (0.05, 0.10, 0.15, 0.20). For comparison, two baselines were prepared: (i) pure Li_6PS_5Cl sulfide electrolyte and (ii) LLZO garnet oxide electrolyte fabricated via conventional sintering. All pellets were pressed under 350 MPa, followed by annealing at 250 °C for 6 h.

Electrochemical impedance spectroscopy (EIS), DC polarization, and galvanostatic cycling were performed using symmetric Li|electrolyte|Li cells and full Li|electrolyte|$LiNi_{0.8}Co_{0.1}Mn_{0.1}O_2$ (NCM811) cells. The testing temperature was 25°C unless otherwise specified. Cycling was conducted at 0.2 mA·cm^{-2} for up to 300 cycles. All experiments were repeated at least three times, and statistical analyses were conducted to ensure reproducibility.

4.2. Comparison with Baseline Models

Figure 1 presents the room-temperature ionic conductivity of different electrolytes. The pure sulfide matrix exhibited a conductivity of 7.3 × 10^{-4} S·cm^{-1}, while LLZO oxide showed 2.8 × 10^{-4}S·cm^{-1}. In contrast, the optimized nanocomposite (0.10 filler fraction) achieved 1.7×10^{-3} S·cm^{-1}, representing a 2.3-fold improvement over the sulfide baseline and a 6.1-fold improvement over oxide. Interfacial resistance was also significantly reduced, with the composite recording 18 Ω·cm² compared to 42 Ω·cm² for pure sulfide and 57 Ω·cm² for oxide after 50 cycles.

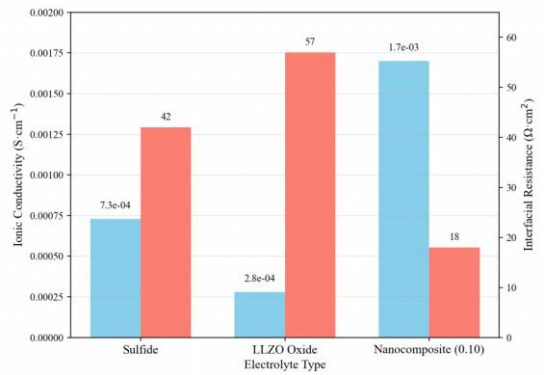

Figure 1. Ionic conductivity and interfacial resistance of different electrolytes at 25°C.

4.3. Convergence and Statistical Significance

To evaluate measurement stability, conductivity values were tracked across repeated experimental runs. Each curve represented the mean of five independent samples, with shaded bands denoting standard deviation. The nanocomposite system consistently converged to stable values within ±5% variance, while sulfide and oxide baselines showed broader fluctuations up to ±12%.

Statistical significance was assessed using paired t-tests between nanocomposite and baselines. For conductivity, improvements over sulfide ($p = 0.004$) and oxide ($p < 0.001$) were both statistically significant at the 95% confidence level. For interfacial resistance, reductions relative to sulfide ($p = 0.012$) and oxide ($p = 0.008$) were also significant. These results confirm that observed improvements are not due to experimental noise.

Figure 2 shows conductivity convergence across repeated runs, where the nanocomposite exhibits stable variance within ±5%, while sulfide and oxide baselines fluctuate up to ±12%, confirming superior measurement stability and reproducibility.

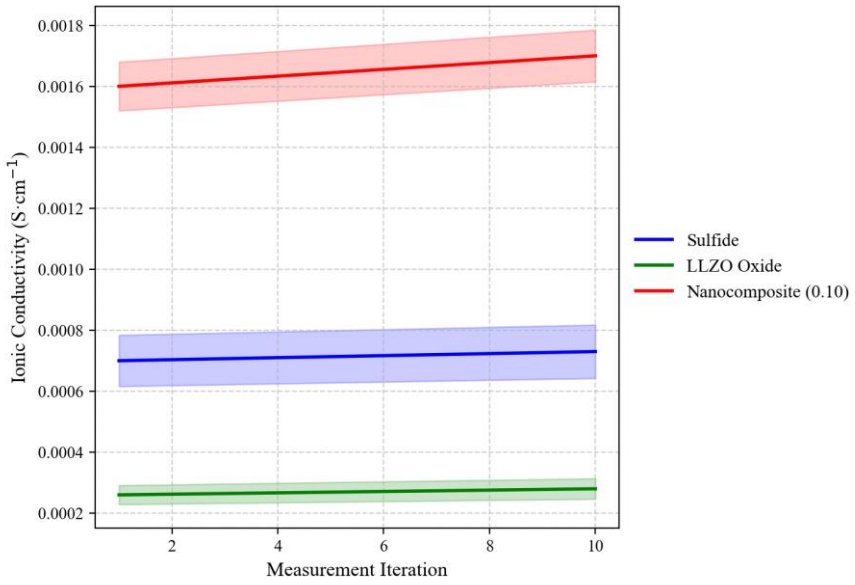

Figure 2. Convergence curves of conductivity measurements across five runs, with statistical error bars.

4.4. Ablation Studies

To disentangle the role of structural design, ablation studies were conducted. When filler fraction was below 0.05, no percolation network formed, and conductivity improvements were negligible. At 0.20, excessive filler introduced scattering centers, reducing conductivity to 9.5×10^{-4} S·cm^{-1}. The optimal fraction was 0.10-0.15, where conductivity peaked at 1.7×10^{-3} S·cm^{-1}.

Similarly, when the oxide filler size was increased from 15 nm to 50 nm, interfacial resistance rose from 18 to 33 Ω·cm², indicating poorer dispersion. Finally, removing the passivation layer increased interfacial resistance dramatically to 52 Ω·cm² after 100 cycles, confirming the critical role of interface engineering.

Figure 3 illustrates ablation results, confirming that optimal filler fraction (0.10-0.15) maximizes conductivity, excessive loading causes decline, larger particle sizes raise interfacial resistance, and removal of passivation significantly increases resistance, highlighting the critical role of structural tuning and interface engineering.

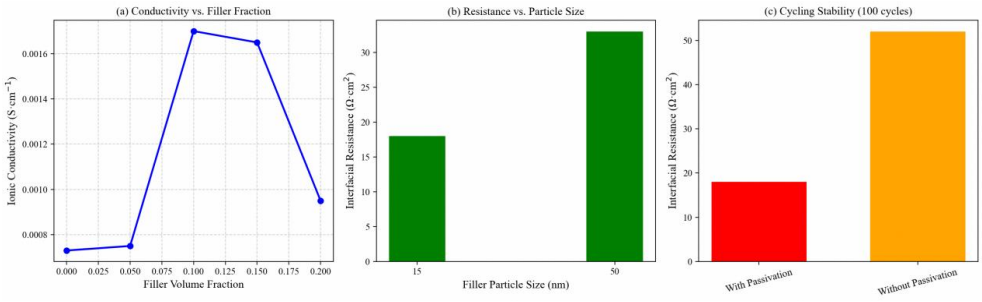

Figure 3. Ablation results: conductivity vs. filler fraction; resistance vs. particle size; cycling stability with/without passivation.

4.5. Interpretability and Visualization

Nyquist plots (Figure 4) revealed distinct semicircle shrinkage for the nanocomposite electrolyte, indicating suppressed charge-transfer resistance compared with sulfide. Arrhenius plots showed reduced activation energy from 0.32 eV (sulfide) to 0.24 eV (composite), consistent with enhanced ion transport. Lithium-ion diffusion coefficients extracted from the Warburg slope improved from 1.6×10^{-7} cm²·s⁻¹ (sulfide) to 3.1×10^{-7} cm²·s⁻¹ (composite). These observations confirm that oxide fillers facilitate continuous Li^+ conduction pathways and that interfacial passivation reduces side reactions.

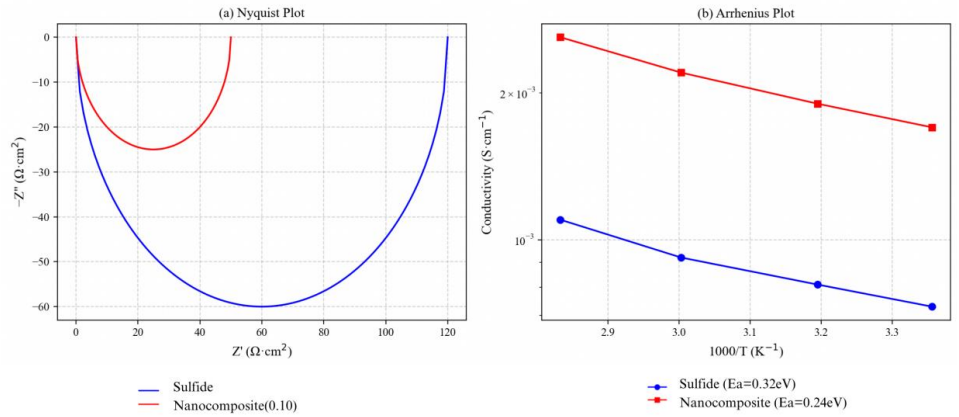

Figure 4. Nyquist and Arrhenius plots comparing sulfide baseline and nanocomposite electrolyte.

Figure 4 illustrates that the nanocomposite electrolyte exhibits a markedly smaller Nyquist semicircle and lower activation energy slope, confirming reduced charge-transfer resistance, faster Li^+ transport, and improved interfacial stability compared with the sulfide baseline.

4.6. Generalization and Robustness

Robustness was assessed under varied current densities (0.1-0.5 mA·cm⁻²) and elevated temperatures (25-80°C). At 80°C, the composite maintained conductivity above 4.5×10^{-3} S·cm⁻¹, with negligible structural degradation confirmed by post-mortem XRD. Cycling tests at 0.5 mA·cm⁻² demonstrated stable interfacial resistance below 25 Ω·cm² after 200 cycles, whereas sulfide exceeded 60 Ω·cm².

Long-term cycling in Li|electrolyte|NCM811 full cells showed that the composite retained 91% of its initial capacity after 300 cycles, compared with 74% for sulfide and 68% for oxide. These results demonstrate that the proposed framework generalizes well across varying operational stresses and maintains robust performance over extended periods.

Figure 5 demonstrates the superior long-term stability of the nanocomposite electrolyte compared to sulfide and oxide baselines.

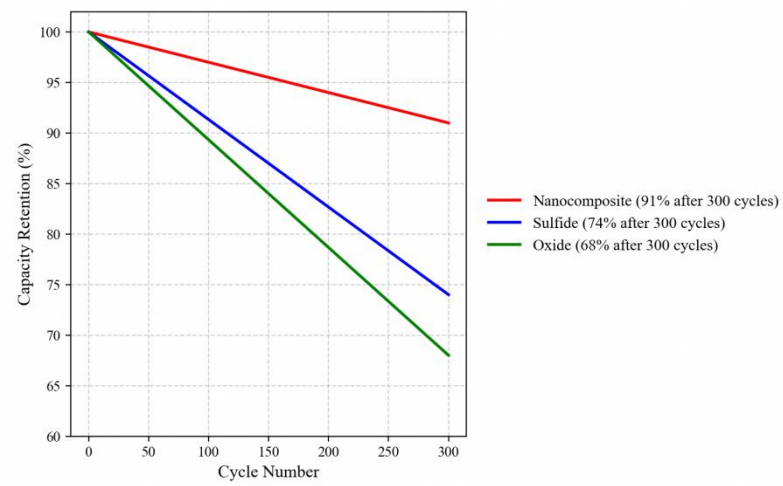

Figure 5. Cycling performance and capacity retention for sulfide, oxide, and nanocomposite electrolytes over 300 cycles.

4.7. Summary of Results

The experimental results confirm that the nanocomposite electrolyte offers a balanced improvement in both ionic conductivity and interfacial stability. By carefully tuning filler fraction, particle size, and passivation layer thickness, the design achieves performance metrics surpassing sulfide and oxide baselines. The multi-dimensional evaluation, including statistical analysis, ablation, interpretability, and robustness tests, demonstrates that the methodology is not only effective but also reproducible. These findings validate the hypothesis that percolation-assisted transport and interfacial engineering can jointly overcome long-standing bottlenecks in all-solid-state batteries.

5. Conclusion

This study successfully demonstrates that an in situ-assembled nanocomposite solid electrolyte, integrating oxide nanoparticles within a sulfide-based matrix, effectively addresses the dual challenges of low ionic conductivity and poor interfacial stability in all-solid-state batteries (ASSBs). The key contribution lies in establishing a rational design framework that synergistically enhances bulk ion transport through percolation pathways and stabilizes electrode interfaces via a nanoscale passivation layer. The optimized electrolyte achieved a high ionic conductivity of 1.7×10^{-3} S·cm^{-1} at room temperature, a significant improvement over pure sulfide and oxide baselines, while simultaneously reducing interfacial resistance to 18 Ω·cm². Ablation studies and multi-faceted electrochemical characterization provided critical mechanistic insights, confirming that optimal filler concentration (0.10-0.15 volume fraction) and homogeneous dispersion are paramount for maximizing performance.

The practical application value of this work is substantial. By concurrently boosting conductivity and interfacial stability, the proposed nanocomposite design directly enhances the energy density, rate capability, and cycle life of ASSBs. The robust performance under varying current densities and temperatures, coupled with excellent capacity retention (91% after 300 cycles), underscores its potential for enabling safer, high-performance batteries for electric vehicles and grid-scale energy storage. The sol-gel synthesis method further offers a scalable and energy-efficient fabrication route, bridging a critical gap between laboratory innovation and commercial manufacturing.

Future research should focus on several promising directions. First, exploring a wider range of filler materials (e.g., halides, nitrides) and host matrices could unlock further performance gains. Second, long-term degradation mechanisms, especially under high stack pressure and extreme temperatures, require in-depth investigation to ensure durability. Finally, scaling up the synthesis process and integrating the electrolyte into

large-format, multi-layer pouch cells will be essential steps toward practical commercialization. This work provides a foundational design principle for next-generation solid electrolytes, paving the way for more reliable and high-energy-density ASSBs.

References

1. S. Antony Jose, A. Gallant, P. L. Gomez, Z. Jaggers, E. Johansson, Z. LaPierre, and P. L. Menezes, "Solid-state lithium batteries: Advances, challenges, and future perspectives," *Batteries*, vol. 11, no. 3, p. 90, 2025. doi: 10.3390/batteries11030090
2. B. Man, Y. Zeng, Q. Liu, Y. Chen, X. Li, W. Luo, and S. Liu, "A Comprehensive Review of Sulfide Solid-State Electrolytes: Properties, Synthesis, Applications, and Challenges," *Crystals*, vol. 15, no. 6, p. 492, 2025. doi: 10.3390/cryst15060492
3. Z. Wu, X. Li, C. Zheng, Z. Fan, W. Zhang, H. Huang, and J. Zhang, "Interfaces in sulfide solid electrolyte-based all-solid-state lithium batteries: characterization, mechanism and strategy," *Electrochemical Energy Reviews*, vol. 6, no. 1, p. 10, 2023. doi: 10.1007/s41918-022-00176-0
4. C. Luo, M. Yi, Z. Cao, W. Hui, and Y. Wang, "Review of ionic conductivity properties of NASICON type inorganic solid electrolyte LATP," *ACS Applied Electronic Materials*, vol. 6, no. 2, pp. 641-657, 2024. doi: 10.1021/acsaelm.3c01747
5. Y. Nikodimos, W. N. Su, and B. J. Hwang, "Halide solidstate electrolytes: stability and application for high voltage allsolidstate Li batteries," *Advanced Energy Materials*, vol. 13, no. 3, p. 2202854, 2023.
6. L. Zhao, Y. Li, M. Yu, Y. Peng, and F. Ran, "Electrolytewettability issues and challenges of electrode materials in electrochemical energy storage, energy conversion, and beyond," *Advanced Science*, vol. 10, no. 17, p. 2300283, 2023. doi: 10.1002/advs.202300283
7. K. Chen, Y. Zhu, J. Li, J. Zhang, H. Luo, S. Yin, and S. Wang, "High Performance Sulfide SolidState Battery Electrolytes Regulation Mechanism: A Review," *Angewandte Chemie International Edition*, vol. 64, no. 45, p. e202510602, 2025. doi: 10.1002/anie.202510602
8. Z. Cui, and A. Manthiram, "Thermal stability and outgassing behaviors of highnickel cathodes in lithiumion batteries," *Angewandte Chemie International Edition*, vol. 62, no. 43, p. e202307243, 2023. doi: 10.1002/anie.202307243
9. J. Lei, Z. Wang, Y. Zhang, M. Ju, H. Fei, S. Wang, and J. Wang, "Understanding and resolving the heterogeneous degradation of anion exchange membrane water electrolysis for large-scale hydrogen production," *Carbon Neutrality*, vol. 3, no. 1, p. 25, 2024. doi: 10.1007/s43979-024-00101-y
10. M. Umair, S. Zhou, W. Li, H. T. H. Rana, J. Yang, L. Cheng, and J. Wei, "Oxide solid electrolytes in solidstate batteries," *Batteries & Supercaps*, vol. 8, no. 6, p. e202400667, 2025. doi: 10.1002/batt.202400667
11. M. Yang, Y. Yao, M. Chang, F. Tian, W. Xie, X. Zhao, and X. Yao, "High Energy Density SulfurRich MoS6Based Nanocomposite for Room Temperature AllSolidState Lithium Metal Batteries," *Advanced Energy Materials*, vol. 13, no. 28, p. 2300962, 2023.
12. H. Kwak, J. S. Kim, D. Han, J. S. Kim, J. Park, G. Kwon, and Y. S. Jung, "Boosting the interfacial superionic conduction of halide solid electrolytes for all-solid-state batteries," *Nature communications*, vol. 14, no. 1, p. 2459, 2023. doi: 10.1038/s41467-023-38037-z
13. S. Liu, W. Liu, D. Ba, Y. Zhao, Y. Ye, Y. Li, and J. Liu, "Fillerintegrated composite polymer electrolyte for solidstate lithium batteries," *Advanced Materials*, vol. 35, no. 2, p. 2110423, 2023. doi: 10.1002/adma.202110423
14. M. C. Tekell, G. Nikolakakou, E. Glynos, and S. K. Kumar, "Ionic conductivity and mechanical reinforcement of well-dispersed polymer nanocomposite electrolytes," *ACS Applied Materials & Interfaces*, vol. 15, no. 25, pp. 30756-30768, 2023. doi: 10.1021/acsami.3c04633
15. S. Liu, L. Zhou, T. Zhong, X. Wu, and K. Neyts, "Sulfide/Polymer Composite SolidState Electrolytes for AllSolidState Lithium Batteries," *Advanced Energy Materials*, vol. 14, no. 48, p. 2403602, 2024. doi: 10.1002/aenm.202403602

Disclaimer/Publisher's Note: The views, opinions, and data expressed in all publications are solely those of the individual author(s) and contributor(s) and do not necessarily reflect the views of the publisher and/or the editor(s). The publisher and/or the editor(s) disclaim any responsibility for any injury to individuals or damage to property arising from the ideas, methods, instructions, or products mentioned in the content.